Title:

Rehabilitation drives functional reorganization of intact corticospinal-supraspinal projections following partial spinal cord injury

Abbreviated title:
Rehab drives CST-supraspinal plasticity after SCI

Author Names and Affiliations:
James Bonanno[1,2], Sheel Trivedi[2], Ciara F. O'Brien[2*], Sharna Saha[2], William B.J. Cafferty[2,3]

1. Interdepartmental Neuroscience Program, Yale School of Medicine, New Haven, Connecticut 06511
2. Department of Neurology, Yale School of Medicine, New Haven, Connecticut 06511
3. Department of Neuroscience, Yale School of Medicine, New Haven, Connecticut 06511

Corresponding Author:
William B.J. Cafferty
Department of Neurology, Yale University School, New Haven, Connecticut 06511 Email: william.cafferty@yale.edu

Number of pages: 39
Number of figures: 5
Number of tables, multimedia, 3D models: 0

Word count: Abstract (239), Introduction (572), Discussion (1487)

Conflict of interest statement:
The authors declare no competing financial interests.

Acknowledgements: This work was supported by the National Institutes of Health National Institute of Neurological Disorders and Stroke Grants R01NS121026 and R21NS139481, and Wings for Life 2023-066.

Present Address (if applicable):
* Cold Spring Harbor Laboratory School of Biological Sciences, 1 Bungtown Road, Cold Spring Harbor, New York 11724

Abstract

Spinal cord injury (SCI) disrupts corticospinal tract (CST) connectivity and impairs skilled voluntary movement, yet most human SCIs are anatomically incomplete, allowing spared CST pathways to engage in rehabilitation-mediated plasticity to promote functional recovery. How voluntary rehabilitation engages and reorganizes the supraspinal targets of the intact CST remains incompletely understood. Here, we combined unilateral pyramidotomy (uPyX) in male and female mice with continuous voluntary complex-wheel running to test whether fine motor-dependent rehabilitation drives supraspinal CST plasticity. uPyX mice rapidly resumed wheel running after a transient deficit. In contrast to lesion-only controls, rehabilitation significantly improved skilled forelimb performance on the horizontal ladder rung task. Immunohistochemical c-Fos labeling confirmed that complex-wheel running robustly activated the intact forelimb CST in motor cortex. Whole-brain CST projection mapping using intersectional viral vector tracing revealed targeted supraspinal reorganization localized to medullary motor nuclei. Three nuclei – the lateral paragigantocellular reticular nucleus (LPGi), gigantocellular reticular nucleus, alpha part (GiA), and ventral medullary reticular nucleus (MdV) – exhibited significant lesion- and/or rehabilitation-induced increases in CST innervation. Rehabilitation-driven CST sprouting correlated with regional c-Fos activation, indicating activity-dependent remodeling. Notably, CST projection density in the MdV, critical for skilled forelimb control, predicted functional recovery. These findings identify a set of spinally-projecting medullary nuclei as key substrates for rehabilitation-induced CST plasticity and highlight the MdV as a potential mediator of restored motor function. This work defines how voluntary rehabilitation reorganizes spared corticospinal pathways and provides targets for optimizing activity-based interventions after SCI.

Significance Statement

Effective rehabilitation after spinal cord injury (SCI) must harness the plasticity of spared motor pathways, yet the supraspinal circuits that support rehabilitation-mediated recovery remain unknown. Using a model that preserves voluntary motor engagement, we show that continuous fine motor-dependent rehabilitation activates intact corticospinal neurons and drives highly specific remodeling of their supraspinal terminals. Rehabilitation selectively strengthens CST inputs to motor regions of the medulla, particularly the ventral medullary reticular nucleus (MdV), and CST plasticity within this region predicts enhanced behavioral recovery. These findings highlight the MdV as a central locus by which rehabilitation re-establishes descending control of the impaired limb, providing mechanistic insight to guide targeted, circuit-based rehabilitation therapies for incomplete SCI.

Introduction

Spinal cord injury (SCI) causes devastating and often permanent loss of voluntary and fine motor control (Mensah et al., 2025). However, most human SCIs are anatomically incomplete, leaving spared motor pathways that can support a limited degree of spontaneous functional recovery (Raineteau and Schwab, 2001; Burns et al., 2012). Currently, intensive rehabilitation is the only established means of enhancing functional recovery in both humans (Lee and Jeoung, 2023) and animal models (Battistuzzo et al., 2012), and emerging evidence indicates that combining it with neuromodulation may further engage spared circuits and strengthen activity-dependent plasticity (Asboth et al., 2018; Wagner et al., 2018). Because adult nervous system axons are unable to regenerate (Liu et al., 2006), rehabilitation is thought to promote functional recovery through neuroplasticity of spared circuits in the brain and spinal cord (Loy and Bareyre, 2019), but the exact anatomical substrates that enable rehabilitation-induced recovery are still poorly understood.

One key target for understanding rehabilitation-induced functional recovery is the corticospinal tract (CST). Located across layer 5 of the sensorimotor cortex, the CST is the primary descending motor pathway that drives voluntary, fine-motor control in mammals (Iwaniuk and Whishaw, 2000; Lemon and Griffiths, 2005). Evidence strongly demonstrates that the intact motor cortex gains new functional control over affected limbs in animal models of partial SCI (Ghosh et al., 2009; Carmel et al., 2014) and stroke (Lindau et al., 2014). Additionally, in animal models of partial SCI (Weidner et al., 2001; Oudega and Perez, 2012), unilateral stroke (LaPash Daniels et al., 2009), and TBI (Dancause et al., 2005), the CST exhibits a capacity for sprouting in the spinal cord and supraspinal motor regions. This sprouting can be enhanced by acute electrical stimulation of the motor cortex (Brus-Ramer et al., 2007), genetic

111 manipulations (Cafferty and Strittmatter, 2006; Lindau et al., 2014), and motor rehabilitation
112 (Starkey et al., 2011; Liu et al., 2016). Moreover, supraspinal motor cortex activation when
113 coordinated with spinal activation leads to enhanced motor outcomes after injury (Van
114 Steenbergen et al., 2022). Together, these studies suggest that activity-dependent plasticity of the
115 CST, driven by rehabilitation, can be leveraged to improve functional recovery from SCI.

116 Recently, data from our laboratory (Golan et al., 2023) and others (Nelson et al., 2021;
117 Carmona et al., 2024) have highlighted and characterized the breadth of CST-supraspinal
118 projections. Specifically, we have identified that the striatum, thalamus, midbrain, pons, and
119 medulla receive input from the CST. While the ventral medulla has previously been identified as
120 a region that undergoes rehabilitation-induced plasticity from the CST (Asboth et al., 2018), a
121 brain-wide investigation of how intact CST-supraspinal terminals reorganize after injury and
122 rehabilitation has never been performed.

123 Here, we used a unilateral pyramidotomy (uPyX) model combined with continuous
124 voluntary fine-motor rehabilitation, whole-brain projection and c-Fos mapping to test whether
125 rehabilitation drives supraspinal remodeling of the intact CST. We find that rehabilitation
126 enhances skilled motor recovery and increases lesion-induced sprouting in motor regions of the
127 medulla. Crucially, we found that intact CST projections in spinally-projecting regions of the
128 motor medulla reorganize in rehabilitated animals in an activity-dependent manner. Finally, we
129 identified three subnuclei of the motor medulla that undergo rehabilitation-induced sprouting and
130 found that sprouting in the ventral part of the medullary reticular formation correlates with
131 improved functional recovery. These insights into the circuit mechanisms by which voluntary
132 rehabilitation reorganizes spared corticospinal pathways lay the groundwork for developing

targeted interventions that amplify rehabilitation-driven plasticity and improve motor outcomes following central nervous system injury.

156 **Materials and Methods**

157 *Mice*

158 C57BL/6 mice (The Jackson Laboratory, Charles River Laboratory) were used for all behavioral
159 and anatomical experiments. The mice were maintained in a temperature and humidity-
160 controlled room on a 12 h light/dark cycle with lights on from 7:00 A.M. to 7:00 P.M with *ad-*
161 *libitum* access to food and water. For experiments, mice were randomly assigned to groups.

162

163 *Surgery*

164 All procedures and postoperative care were performed in accordance with the guidelines of the
165 Institutional Animal Use and Care Committee at Yale University.

166

167 *Unilateral Pyramidotomy (uPyX):* Mice received a left side unilateral pyramidotomy in the
168 medulla rostral to the pyramidal decussation as previously described (Cafferty & Strittmatter,
169 2006). Briefly, mice were anesthetized with ketamine (100 mg/kg) and xylazine (15 mg/kg) and
170 placed in a supine position, an incision was made to the left of the trachea, and blunt dissection
171 exposed the occipital bone at the base of the skull. Depth of anesthesia was continuously
172 monitored via reflexes and depth of breath. The occipital bone was removed on the left side of
173 the basilar artery with blunt Dumont #2 forceps to expose the medullary pyramids. The dura
174 mater was pierced with a 30-gauge needle and resected. The left pyramid was transected
175 unilaterally with fine Dumont #5 forceps to a depth of 0.25 mm or exposed for sham lesion. No
176 internal sutures were made, and skin was closed with monofilament suture. All animals received
177 pre-surgical analgesia (Buprenorphine extended release 3.25 mg/kg subcutaneously), and post-
178 surgical antibiotics (Ampicillin, 100 mg/kg subcutaneously) for 2 days post lesion. Histological

179 verification of lesion completeness was performed after the completion of behavioral
180 experiments using PKC gamma staining of cervical spinal sections (Cell Signaling Technology,
181 #59090).
182
183 *Intersectional CSN Labeling:* Intersectional viral tracing was completed at day 28 post lesion to
184 ensure no tracing dependent functional deficits contributed to behavioral assessments. To label
185 forelimb CSNs, adult mice were anesthetized with ketamine (100 mg/kg; Covetrus) and xylazine
186 (15 mg/kg; Covetrus) and placed in a stereotaxic frame (Stoelting). First, a small incision was
187 made into the skin and retracted using hemostats. Small craniotomies were then made over the
188 centers of mouse rostral forelimb area (RFA), coordinates +2.0-2.5 mm AP and +0.5-1.5 mm
189 ML from bregma, and caudal forelimb area (CFA), coordinates -0.5-1.0 mm AP and +1.0-1.5
190 mm ML from bregma. The tip of a pulled glass capillary tube attached to a 5 µl Hamilton syringe
191 was loaded into a Micro4 infusion device (World Precision Instruments) for a total of two
192 injections of pAAV1-CAG-FLEX-eGFP (Addgene, #59331) into RFA and three injections of
193 pAAV1-FLEX-tdTomato (Addgene, #28306) into CFA at a depth of 500 µm. Each injection site
194 received a total of 100 nL of virus at a rate of 40 nL/min. After each injection, the capillary tube
195 was kept in place for 30 sec before being pulled up slowly. After all injections were completed,
196 the skin was sutured with 4.0 Vicryl (McKesson) and mice prepared for spinal injections.
197 During the same procedure, an incision was made over the cervical enlargement to reveal
198 C5-C8 vertebrae by first dissecting overlying muscle. Then, a unilateral left side laminectomy
199 was performed to expose the underlying spinal cord. The same injection apparatus was used for
200 spinal injections. For each spinal level in the C5-C8 range, the capillary tube was slowly inserted
201 stereotaxically to a depth of 500 µm into the spinal cord and ~600 µm lateral from the midline.

202 30 seconds after the introduction of the capillary tube, 100 nL of pENN-rAAV-.hSyn-Cre-
203 WPRE-hGH (Addgene, catalog #105553) was infused into the spinal cord over 2 min. The tip
204 was left *in situ* for an additional 30 sec before removal. After all injections, the skin was sutured
205 with 4.0 Vicryl, and mice were monitored until they awoke from anesthesia. All animals
206 received pre-surgical analgesia (Buprenorphine extended release 3.25 mg/kg subcutaneously),
207 and post-surgical antibiotics (Ampicillin, 100 mg/kg subcutaneously) for 2 days post lesion.
208
209 *Voluntary Complex Wheel Running Rehabilitation:* Voluntary rehabilitation was administered to
210 mice (2–3 months old, n = 9 males, 13 females) using our previously described REVS hardware
211 and software system (Bonanno et al., 2025). Briefly, mice randomly assigned to rehabilitation
212 groups were given access to running wheels for five days prior to lesion for habituation. This
213 included two days of regular wheels, followed by three days of complex wheels. Regular wheels
214 had 1 cm rung separations and complex wheels had a mix of 1-3 cm rung separations. Mice had
215 access to running wheels 24 hours a day, except for the 48 hours immediately after the
216 lesion/sham surgery. Mice (n=1, uPyX+Rehab) that failed to engage in wheel running were
217 removed from the study and excluded from analyses. Wheels were cleaned with water and
218 ethanol once a week after ladder rung testing.
219
220 *Complex Ladder Rung:* Mice (2–3 months old, n = 27 males, 18 females) were trained for
221 forepaw and hind paw dexterity assessment using an irregular horizontal ladder. Mice were
222 handled for 3 days prior to any behavioral testing and were allowed to habituate to the ladder
223 apparatus with regularly spaced rungs for 5 minutes. After habituation, mice were trained to
224 cross the regular ladder to a safe box with bedding. A bright light was placed at the start of the

225 ladder to encourage crossing to the safe box. Experimental handling was carried out by an
226 experimenter blinded to lesion status. A GoPro Hero8, set up 7.5 inches from the apparatus, was
227 used to capture video recordings of performance on the irregular ladder rung (Metz and
228 Whishaw, 2009) at baseline and 2-, 7-, 14-, 21-, and 28- days post lesion. Rungs were spaced 1,
229 2, or 3 cm apart in a randomized pattern which was changed between testing sessions to prevent
230 learning. In an individual behavior session, mice crossed the irregular ladder three times,
231 resulting in a total of 1 meter of distance traveled.

232 To analyze paw placement as an injury metric, first DeepLabCut (Mathis et al., 2018)
233 was used to track performance of the forepaws and hind paws for each mouse. A network with
234 300 frames, selected from a random mix of sham and lesioned animals across all days, was
235 trained and refined until predictions were less than 5 pixels off compared to human-labeled
236 frames. A total of 166 videos were analyzed using the network. Videos were manually
237 preprocessed for DeepLabCut by cutting out frames without the mouse. Output CSV files were
238 processed and analyzed using a custom-written peak detection algorithm in R to detect missed
239 steps using paw y-position. A cut-off was set to count any placement of the paw below the center
240 of each rung as a missed step. Total number of missed steps calculated for each limb. Injured
241 fore limb reach errors, or overreaches, were quantified by setting a threshold two standard
242 deviations above the mean step height. Cross time was calculated by multiplying total frames by
243 the frame rate of the camera.

244

245 *Immunohistochemistry:* Ten days after intersectional AAV injections, mice were euthanized with
246 isoflurane and transcardially perfused with 0.9% NaCl with 10 units/ml heparin (Covetrus, 1000
247 unit/ml) followed by 4% paraformaldehyde (PFA) in PBS. Brains and spinal cords were

248 dissected and post-fixed in 4% PFA overnight at 4°C. The next day, 75 µm thick sections of
249 brain and 35 µm of cervical spinal cord were cut using a vibratome (Leica microsystems,
250 VT1000S), and sections prepared for free-floating immunohistochemistry.

251 *Corticospinal-supraspinal terminal detection and c-Fos activation*: Every other section
252 throughout the brain was stained using free floating IHC. Sections were washed in 0.2% PBS-T
253 3x and blocked in 10% Normal Donkey (NDS) or Normal Goat Serum (NGS) for 1 hour.
254 Primary antibodies to enhance RFP and GFP signal, Chicken anti-RFP (Abcam; ab13970,
255 RRID:AB_300798) and Rabbit anti-GFP were used (Abcam; ab167453, RRID:AB_2571870) in
256 addition to Guinea Pig anti-c-Fos (Synaptic Systems, 226 308, RRID:AB_2905595) were diluted
257 1:1,000 in PBS-T in 10% serum overnight at RT. The following day, sections were washed 3x in
258 PBS-T, and incubated in secondary antibodies (Alexa Fluor 546: A10040, A32732; Alexa Fluor
259 488: A78948, A32931; Alexa Fluor 647: A21450, ThermoFisher) for 2 hrs. Next, sections were
260 washed 3x in PBS-T. The final wash contained a 1:10,000 dilution of 1 mg/ml DAPI stock
261 solution (ThermoFisher, 62448). Sections were then mounted onto Superfrost Plus slides and
262 treated with TrueBlack (Biotium, 23007) for 30 secs diluted 20x in 70% EtOH to reduce
263 autofluorescence and background staining. Slides were then washed 3x in PBS and cover slipped
264 with Fluoro-Gel (Fisher Scientific, 17985-11). Whole-section imaging at 4x was performed
265 using an Olympus VS200 Slide Scanner.

266 *PKC-γ detection for lesion completeness*: Histological verification of lesion completeness
267 was performed after the completion of behavioral experiments using PKC-γ staining of cervical
268 spinal sections. Cervical spinal sections were washed in 0.2% PBS-T 3x and blocked in 10%
269 Normal Donkey (NDS) for 1 hour. Sections were then incubated with Rabbit anti-PKC-γ (Cell
270 Signaling Technology, #59090) primary antibody overnight at RT. The following day, sections

were washed 3x in PBS-T and incubated in Donkey anti-rabbit Alexa Fluor 647 (A31573, Fisher Scientific) secondary antibodies for 2 hours, then washed 3x in PBS-T and mounted with Fluoro-Gel (Fisher Scientific, 17985-11). Mice were excluded (n=4 uPyX+Rehab, 4 uPyX-Rehab) from the study if lesioned side ventral dorsal column staining was assessed to be 5% or more intact.

BrainJ Projection Density Analysis: BrainJ software was used to label CSN soma and axons projections throughout each brain, as previously described (Botta et al., 2020). Briefly, sections were manually ordered and registered to the Unified Kim Mouse Brain Atlas (Chon et al., 2019) template using Elastix software, version 5.0.1. Next, ilastik, version 1.3.3 was used to identify brainwide soma and projections in the ~75 mounted sections using pixel-based machine learning. Ilastik training was performed by two experimenters blinded to groups. BrainJ output absolute density measurements for 1429 subregions of the brain, as defined by the Kim Atlas. Projection density for each animal was normalized to the total projection density measured in the corticospinal fiber tracts. For higher level projection analysis, we assigned subregions to one of fifteen functional regions: isocortex, striatum, thalamus (sensory-motor), thalamus (other), midbrain (motor), midbrain (sensory), midbrain (other), pons (motor), pons (sensory), pons (other), medulla (motor), medulla (sensory), medulla (other), and cerebellar nuclei.

Experimental Design and Statistical Analysis

Behavioral experiments: There were four groups including both sexes: Sham without rehabilitation (Sham-Rehab, n=8), Sham with rehabilitation (Sham+Rehab, n=7), uPyX without rehabilitation (uPyX-Rehab, n=11), and uPyX with rehabilitation (uPyX+Rehab, n=11). Rehabilitation metrics were collected from rehabilitation groups only using REVS, and those

294 analyzed included total distance, total hours run, and overall speed. Cumulative distance run was
295 separately calculated by summing the total distance per night for each animal. Each
296 rehabilitation metric was evaluated using a mixed-model ANOVA with a between-subjects
297 variable of lesion status and a within-subjects variable of day. Post-hoc t-test comparison of
298 baseline and 2 dpi specifically were performed for each metric to assess acute deficits.
299 For the complex ladder rung task, total injured forelimb steps, injured forelimb footfalls,
300 intact forelimb footfalls, injured forelimb reach errors, injured hindlimb footfalls, and intact
301 hindlimb footfalls were measured to assess fine motor control, and total time to cross was
302 measured as a general metric of impairment. Complex ladder rung metric was assessed using
303 mixed-model ANOVAs with between-subjects variables of lesion status and treatment
304 (rehabilitation) and a within-subjects variable of day. Separate ANOVAs were run for the
305 baseline to 2 dpi time period and the 7 dpi and 28 dpi time periods to isolate the effects of lesion
306 and rehabilitation. When significant main effects were detected, post hoc t-tests were performed
307 to identify specific differences between groups on specific days. Post hoc testing was corrected
308 for multiple comparisons using Bonferroni corrections. A principal component analysis (PCA)
309 was performed on injured forelimb steps, footfalls, reach errors, intact footfalls, injured hindlimb
310 footfalls, intact hindlimb footfalls, and time to cross across -2, 2, and 28.
311
312 *Colocalization analyses*: CSNs and c-Fos positive cells were labeled using ilastik. A list of
313 detected CSNs and c-Fos positive cells, and all channel intensity values for each cell, was output
314 for each brain. The threshold for a CSN to be classified as "positive" was the minimum intensity
315 value of c-Fos detected cells for a given brain. For analyses, CSNs were automatically assigned
316 to M2 and M1 of motor cortex based on the Kim Atlas, and measurements from RFA- and CFA-

317 traced CSNs were included. CSNs assigned to layers 1 and 6 were removed from analyses.
318 Linear mixed-effect models were performed with colocalization proportion as the dependent
319 variable, lesion status and treatment as fixed effects, and subject ID as a random intercept. A
320 subset (n = 12) of mice in the rehabilitation and complex ladder rung experiments received c-Fos
321 staining. For this experiment Sham+Rehab and uPyX+Rehab mice were confirmed to have run
322 within the previous hour using REVs.
323
324 *Projection Density Analyses*: The dependent variable was projection density in a given region, as
325 defined by total signal occupied divided by total region area. Projection density measurements
326 were normalized for each animal (n = 9 control, 5 uPyX-Rehab, 5 uPyX+Rehab) based on the
327 total projection density measured in corticospinal fiber tracts, as measured by BrainJ. Mixed-
328 effect linear models were used for both the higher level (i.e., medulla-motor) and granular (i.e.,
329 MdV) projection density analyses. Mice with failed tracing were excluded from analyses. Lesion
330 status and treatment (rehabilitation) were used as fixed effects in the model, with animal ID
331 included as a random effect. For sub-region analysis, we restricted our analyses to spinally-
332 projecting subregions, as identified by Wang et al., 2022. Post-hoc t-tests were only performed
333 on subregions identified as having significant interactions between region and group. P-values
334 were corrected for multiple comparisons using the Tukey method for adjustment.
335
336 *Plasticity and Rehabilitation Indices*: We computed a "Plasticity Index" by dividing normalized
337 projection density in uPyX-Rehab mice and uPyX+Rehab mice in a given subregion by the
338 average Sham control value. This was correlated with a "Rehabilitation Index", a proxy of
339 rehabilitation-induced c-Fos activation in given subregions, which was calculated by dividing the

average c-Fos density in runners divided by non-runners. Mice were the same as used for co-localization analyses. Only spinally-projecting regions (Wang et al., 2022) were included or these analyses.

Statistical analyses: Statistics were performed in R (version 4.4.1) using base R, lme4Test, and emmeans on blinded experimental groups. Footfalls, reach errors, and cross time were calculated using custom-written code to analyze paw coordinate positions, as tracked by DeepLabCut. No main effects or interactions with sex were observed in any behavioral or anatomical measure, so data from males and females were pooled. For all statistical analyses, an alpha value of 0.05 was selected *a priori*, and p-values were adjusted for multiple comparisons.

362 **Results**

363

364 *Voluntary rehabilitation engagement in uPyX and sham mice*

365 We first asked whether mice with unilateral pyramidotomy (uPyX) would engage in complex-
366 wheel running as a form of voluntary rehabilitation. After wheel habituation, mice received
367 either a unilateral lesion of the left medullary pyramid or a sham surgery and were given access
368 to runged wheels from 2 to 28 days post-injury (dpi) (**Fig. 1A**). Lesions were verified with PKC-
369 γ immunostaining, and animals with incomplete lesions were excluded (**Fig. 1B-C**).

370 Using the REVS platform (**Fig. 1D-F**) we acquired daily wheel running metrics. Across the 4-
371 week rehabilitation period, uPyX and sham mice achieved comparable runtime, speed, and
372 distance (**Fig. 1G-I**). There were no baseline differences observed between groups ($p > 0.25$ for
373 all metrics), however, uPyX animals displayed a significant reduction in runtime, speed, and
374 distance at 2 dpi ($p < 0.01$ for all comparisons), reflecting an acute motor deficit. These
375 impairments resolved rapidly, with performance returning to sham levels by one week of
376 rehabilitation (**Fig. 1G–I**). Mixed-factor ANOVAs confirmed significant time × injury
377 interactions for all running metrics ($p < 0.001$), but no long-term effect of injury on cumulative
378 running ($p = 0.33$, **Fig. 1J**). Thus, uPyX mice fully re-engaged in voluntary complex-wheel
379 running, enabling equivalent total rehabilitation between sham and lesioned mice.

380 *Rehabilitation enhances recovery of skilled forelimb function*

381 To determine whether voluntary rehabilitation improved skilled motor performance, mice were
382 tested on a complex ladder-rung task at baseline and at 2, 7, 14, 21, and 28 dpi (**Fig. 2A–B**). In

383 addition to the uPyX+Rehab and Sham+Rehab groups, non-rehabilitated uPyX and Sham
384 controls were included to isolate the effects of rehabilitation.

385 At 2 dpi, uPyX animals exhibited significant increases in injured forelimb (FL) steps, injured FL
386 footfalls and intact FL footfalls compared with sham controls ($p < 0.05$ for all, ANOVA),
387 confirming a lesion-induced deficit (**Fig. 2C-E**). There was additionally a significant increase in
388 injured FL reach errors ($p < 0.001$, ANOVA) (**Fig. 2F**). Across 7–28 dpi, rehabilitation
389 significantly reduced footfall and reach errors. Both footfall and reaching errors showed main
390 effects of lesion (footfall: $p = 0.001$; reach: $p = 0.002$, ANOVA) and rehabilitation ($p = 0.008$;
391 reach: $p = 0.005$), with post hoc tests revealing that uPyX+Rehab mice improved progressively
392 and reached near-sham levels by 21–28 dpi ($p < 0.05$ vs. uPyX-Rehab). The rehabilitation effect
393 on reaching errors emerged as early as 7 dpi ($p < 0.05$ vs. uPyX-Rehab) and persisted throughout
394 the testing period.

395 The injured and intact hindlimb (HL) also showed lesion effects ($p < 0.05$ for both, ANOVA) but
396 were unaffected by rehabilitation (**Fig. 2G-H**). To visualize group-level behavioral patterns, we
397 performed a principal component analysis (PCA) across all seven metrics (**Fig. 2I-K**). At
398 baseline, all groups clustered together; at 2 dpi, both uPyX groups separated from shams. By 28
399 dpi, uPyX+Rehab mice re-clustered with sham controls, whereas uPyX-Rehab animals remained
400 isolated (**Fig. 2C**). Together, these findings show that voluntary rehabilitation promotes robust
401 and lasting recovery of fine forelimb control after unilateral CST injury.

402 *Complex-wheel running recruits intact corticospinal neurons*

403 We next asked whether voluntary complex-wheel rehabilitation engages spared CSNs. Using
404 intersectional viral tracing, we labeled CSNs originating from the rostral (RFA) and caudal

405 (CFA) forelimb motor cortices and assessed neuronal activation with c-Fos immunostaining (**Fig**
406 **3A**). Mice were euthanized during their active cycle, and rehabilitation animals were confirmed
407 to have run within the previous hour using REVs.

408 CSNs localized to M1 and M2 using the Kim Atlas showed strong c-Fos expression following
409 complex-wheel running, irrespective of their tracing origin, indicating robust recruitment of the
410 intact forelimb CSNs during rehabilitation (**Fig. 3B-G**). Across groups, there was a main effect
411 of rehabilitation (M2: $p = 0.005$, M1: $p = 0.004$), but not lesion (M2: $p = 0.21$; M2: $p = 0.26$).
412 This engagement suggested that the complex-wheel paradigm not only promotes behavioral
413 recovery but also drives activity in spared CSNs.

414 *Rehabilitation drives CST-supraspinal terminal plasticity*

415 Given the recruitment of intact CSNs, we next investigated whether rehabilitation induced
416 supraspinal structural plasticity. Using the same intersectional labeling, we performed whole-
417 brain projection density mapping with BrainJ to quantify CSN projections in 15 functional
418 subregions spanning the cerebrum (blue), interbrain (green), midbrain (purple), pons (orange),
419 medulla (pink), and cerebellum (yellow) (**Fig. 4A**).

420 Projection density patterns were not significantly different between sham animals with or
421 without rehabilitation; therefore, these groups were pooled as controls. Compared with controls,
422 both lesion groups exhibited increased projection density in the motor regions of the medulla
423 (uPyX+Rehab vs. Control, $p < 0.001$; uPyX-Rehab vs. Control, $p = 0.013$), with the largest
424 changes observed in rehabilitated animals (**Fig 4B**). In contrast, non-sensory/motor regions of the
425 isocortex showed decreased density in uPyX+Rehab mice (uPyX+Rehab vs. Control, $p = 0.005$).
426 Thus, rehabilitation induced targeted rather than global CST-supraspinal reorganization, with

427 pronounced effects in brainstem motor nuclei. All other subregions showed no significant
428 difference between groups. Additionally, there was no significant effect of tracing origin on CST
429 projection density.

430 To link neural engagement during rehabilitation to plasticity of intact CST projections, we
431 derived a "rehabilitation index" from regional c-Fos activation and a "plasticity index" from
432 normalized CST projection density relative to controls. Across spinally projecting regions, these
433 indices were significantly correlated in the motor medulla of uPyX+Rehab mice but not in uPyX-
434 Rehab animals (Pearson's correlation; $R^2 = 0.161$, $p = 0.031$), indicating that CST reorganization
435 occurs preferentially in regions most activated during rehabilitation (**Fig. 4C–D**). No such
436 correlation was observed in a control region (motor pons), suggesting region-specific, activity-
437 dependent plasticity (**Fig. 4E–F**).

438 *Rehabilitation-induced plasticity localizes to specific motor medulla nuclei*

439 Because the motor medulla emerged as a major locus of CST reorganization, we next examined
440 projection density at the level of individual medullary nuclei. Mixed-effects models identified
441 three nuclei showing significant lesion- and/or rehabilitation-induced plasticity: the lateral
442 paragigantocellular reticular nucleus (LPGi), the alpha part of the gigantoreticular nucleus (GiA),
443 and the ventral medullary reticular nucleus (MdV) (**Fig. 5A-C).** Projection density increased in
444 the LPGi ($p = 0.010$) and GiA ($p < 0.001$) specifically in uPyX+Rehab animals relative to
445 controls, whereas the MdV exhibited increases in both uPyX-Rehab ($p = 0.004$) and
446 uPyX+Rehab ($p < 0.001$) groups, suggesting contributions from both lesion and rehabilitation
447 (**Fig. 5A–D**). For all three of these subregions, there was no significant effect of tracing origin on

448 CST projection density. Representative images show intact CST projection density in the rostral
449 (**Figs. 5D-G**) and caudal (**Figs. 5H-K**) medulla.

450 Crucially, to determine the functional relevance of these changes, we correlated CST projection
451 density in each nucleus with behavioral recovery. Projection density in the MdV, but not LPGi or
452 GiA, significantly correlated with improved forelimb footfall recovery (Pearson's correlation; R^2
453 = 0.327, p = 0.011; **Figs. 5D–F**). These findings reveal the MdV as a key nucleus where intact
454 CST structural plasticity is directly linked to functional improvement.

455

456

457

458

459

460

461

462

463

464

465

466 **Discussion**

467 Here, we show that voluntary, fine motor-dependent rehabilitation drives robust recovery of
468 skilled forelimb function after partial CST injury and induces highly targeted CST-supraspinal
469 terminal plasticity. By combining uPyX with continuous complex-wheel training and whole-
470 brain projection mapping, we identify specific medullary reticular nuclei that undergo
471 rehabilitation-dependent CST remodeling and link this structural plasticity to functional
472 activation and behavioral recovery. These results provide new insight into how voluntary motor
473 rehabilitation engages and reorganizes intact supraspinal pathways to support functional recovery
474 after SCI.

475

476 *Voluntary rehabilitation drives recovery of skilled motor function*

477 Recovery of motor function after SCI is dependent in part on the capacity of spared,
478 descending tracts to reorganize and reintegrate with impaired motor circuits (Fink and Cafferty,
479 2016) . Motor rehabilitation of the affected limbs is key to this process in humans (Lee and
480 Jeoung, 2023) and rodent models (Mensah et al., 2025). However, the anatomical mechanisms
481 through which rehabilitation promotes functional recovery are unknown. Despite significant
482 damage to descending motor pathways, human SCIs are rarely anatomically complete (Burns et
483 al., 2012), allowing residual motor circuits to serve as substrates for activity-dependent re-wiring
484 via rehabilitation. This underscores the need for models that promote sustained motor
485 engagement after SCI.

486 Here, we established a voluntary rehabilitation model that maintains high levels of motor
487 activity after partial CST injury. The unilateral pyramidotomy model (uPyX) results in a specific
488 unilateral lesion to the CST while preserving other sensorimotor pathways. This allows animals

489 to retain gross locomotor function yet display reproducible fine motor deficits (Starkey et al.,
490 2011). Thus, the uPyX model is well suited for studying activity-dependent recovery of fine
491 motor function and plasticity in spared corticospinal circuits.

492 Using our REVS platform (Bonanno et al., 2025) for continuous wheel-running
493 monitoring, we confirmed that uPyX mice engaged in sustained, self-directed wheel running
494 throughout the rehabilitation period (**Fig. 1**). To selectively engage the CST for fine motor
495 control (Iwaniuk and Whishaw, 2000), we used complex rung-patterned wheels. Consistent with
496 previous work showing that lesioned animals can attain sham levels of wheel running shortly
497 after injury (Loy et al., 2018), we found that uPyX mice quickly restored their capacity for
498 complex, voluntary wheel running (**Fig. 1**). This indicates that spared CST circuits remain highly
499 recruitable after uPyX, providing a foundation for recovery of skilled motor function and
500 rehabilitation-induced plasticity. Indeed, voluntary rehabilitation led to significant improvement
501 of functional forelimb metrics, with rehabilitated mice achieving sham-level accuracy on the
502 complex ladder rung task within 1-3 weeks post-injury (**Fig. 2**). Recovery of forelimb footfalls
503 and forelimb reach errors is consistent with the restoration of typical corticospinal control and
504 suggests that rehabilitation led to more than just gross locomotor improvements.

505 Notably, prior studies show that reach training rehabilitation paradigms induce task-
506 specific recovery but impair performance on untrained tasks including the complex ladder rung
507 task (Girgis et al., 2007; Krajacic et al., 2010). By contrast, voluntary complex-wheel running
508 here led to task non-specific improvements that generalized to the complex ladder rung task.
509 This suggests that high levels of CST-targeted voluntary motor training may facilitate more
510 general restoration of forelimb function. Overall, these findings validate our model as suitable

511 for studying rehabilitation-induced functional recovery after partial SCI and motivate an
512 investigation of how voluntary rehabilitation recruits spared corticospinal pathways.
513
514 *Mechanisms of Voluntary Rehabilitation-Driven Plasticity in Spared Corticospinal Circuits*
515 We found that voluntary complex-wheel running increased c-Fos expression in intact
516 CSNs from M1 and M2 of forelimb motor cortex (**Fig. 3**), confirming that rehabilitation engages
517 intact CST pathways which are critical for skilled motor control after injury (Carmel et al., 2010;
518 Wahl et al., 2014). Moreover, this neural recruitment can facilitate activity-dependent plasticity
519 in spared CSN circuits, which have previously been described to functionally reorganize after
520 injury and rehabilitation (Weidner et al., 2001; Dancause et al., 2005; Ghosh et al., 2009).
521 Whole-brain projection mapping revealed that rehabilitation-induced intact CST
522 structural remodeling is highly targeted to specific supraspinal brain regions. Significant
523 increases in CST projection density were localized to the motor-medulla, specifically the lateral
524 paragigantocellular nucleus (LPGi), the alpha part of the gigantoreticular nucleus (GiA), and the
525 ventral medullary reticular nucleus (MdV). We did not detect a difference in RFA- and CFA-
526 traced projection density for these three regions, consistent with a previous report showing
527 similar innervation patterns by RFA- and CFA-CSNs throughout the motor medulla (Carmona et
528 al., 2024). In contrast, the non-sensorimotor isocortex showed reduced CST projection density
529 after rehabilitation, suggesting a pruning or reorganization of projections away from less
530 functionally relevant targets (Kleim and Jones, 2008).
531 Novelly, we found that the extent of CST plasticity within medulla subregions strongly
532 correlated with the level of neuronal activation induced by rehabilitation in those same regions
533 (**Fig. 4**). This supports a model of rehabilitation-induced region-specific functional

534 reorganization, in which rehabilitation selectively strengthens intact projections to circuits most
535 engaged by fine motor control. Consistent with this model, studies have demonstrated that CST
536 collateral sprouting and synaptogenesis is dependent on post-synaptic partner activity and
537 signaling (Ueno et al., 2012; Bradley et al., 2019).

538 The medullary reticular nuclei which underwent CST remodeling here have distinct,
539 complementary roles in fine motor control (Inoue and Ueno, 2025). The MdV is critical for
540 skilled forelimb function such as grasping (Esposito et al., 2014). In line with this functional
541 role, intact CST projection density in this subregion correlated with forelimb footfall percentage
542 recovery (**Fig. 5**). The LPGi and GiA primarily contribute to speed modulation and locomotion
543 initiation (Capelli et al., 2017; Zhang et al., 2024). While we observed *de novo*, rehabilitation-
544 specific increases in CST density in these regions, CST density here did not correlate with
545 forelimb footfall recovery. Nevertheless, rehabilitation-induced sprouting in these regions may
546 play a supporting role in reorganizing motor control networks to re-establish the skilled motor
547 function observed in rehabilitated mice. Additionally, plasticity in these nuclei may play a more
548 consequential role in functional recovery after more severe SCI (Lemieux et al., 2024).

549 The MdV, LPGi, and GiA project predominantly ipsilaterally to the spinal cord (Esposito
550 et al., 2014; Liang et al., 2016), positioning these nuclei to convey descending motor commands
551 to the denervated side after unilateral injury. This ipsilateral organization creates a substrate
552 through which spared CST axons can reroute motor output via reticulospinal pathways to the
553 denervated spinal circuits. Crucially, these reticulospinal circuits are often spared after contusion
554 injury (Wang et al., 2022).

555 Previous work has highlighted the importance of plasticity within descending
556 reticulospinal and midbrain pathways (Filli et al., 2014; Lemieux et al., 2024; Jeleva et al.,

557 2026). Our findings extend this framework by demonstrating that rehabilitation also induces
558 plasticity of corticospinal inputs onto these same brainstem nuclei. This finding aligns with the
559 established role of the CST in modulating both supraspinal and spinal motor circuits in intact and
560 injured states (Liu et al., 2018; Ueno et al., 2018; Moreno-Lopez et al., 2021; Glover and Baker,
561 2022). Moreover, after injury, CST axons have been shown to form detour circuits through
562 propriospinal and brainstem relays (Bareyre et al., 2004; Asboth et al., 2018), providing support
563 for the cortico-reticular remodeling observed here.

564 Our study builds upon the cortico-reticular model proposed by Asboth et al., 2018.
565 Firstly, we show that CST projections, rather than intratelencephalically-projecting motor neuron
566 projections, undergo terminal plasticity. Secondly, we identify the specific medullary subregions
567 of the reticular formation that are modulated in rehabilitated mice. Finally, we demonstrate that
568 there are unique patterns of sprouting amongst these different reticulospinal sub-regions (i.e,
569 MdV experienced uPyX-Rehab and uPyX+Rehab sprouting, while LPGi/GiA only experienced
570 uPyX+Rehab sprouting).

571 Together, our findings support a model in which rehabilitation selectively promotes CST
572 sprouting toward medullary nuclei that are anatomically and functionally poised to re-establish
573 descending control of the impaired limb.

574

575

576 *Limitations and Future Directions*

577 While our rehabilitation intervention was causally linked to improvements in motor
578 behavior, anatomical analyses of the intact CST presented here are correlational and do not by
579 themselves establish that CST sprouting within the motor medulla directly drives recovery.
580 Nevertheless, we believe that the strong association between CST projection density in the MdV

581 and functional improvement suggests a potential causal contribution that warrants further testing.
582 Indeed, our previous data showed that chemogenetic silencing of lesion-induced sprouting of
583 rubro-raphe circuits abrogated recovery of fine forelimb function after bilateral pyramidotomy
584 (Siegel et al., 2015). The present work provides a foundation for similar studies using region-
585 specific circuit manipulation to directly determine the role of corticospinal–medullary pathways
586 in mediating rehabilitation-induced recovery across various SCI models.

587 A second consideration is the translational relevance of the uPyX model. Although it
588 most closely resembles partial lesions such as Brown–Séquard syndrome and unilateral cortical
589 stroke, its primary advantage is its ability to isolate the capacity for CST reorganization, which
590 ultimately uncovered three specific medullary nuclei associated with rehabilitation-induced
591 recovery. Finally, the molecular and cellular mechanisms that govern CST-supraspinal
592 remodeling remain incompletely defined. Elucidating these mechanisms and determining how
593 targeted rehabilitation paradigms might selectively engage homologous cortico-reticular systems
594 in humans, represents a key step toward optimizing activity-based therapies to enhance
595 functional recovery after SCI.

596

597

598

599

600

601

602 **References**

603 Asboth L, Friedli L, Beauparlant J, Martinez-Gonzalez C, Anil S, Rey E, Baud L, Pidpruzhnykova G,
604 Anderson MA, Shkorbatova P, Batti L, Pagès S, Kreider J, Schneider BL, Barraud Q, Courtine G
605 (2018) Cortico-reticulo-spinal circuit reorganization enables functional recovery after severe spinal
606 cord contusion. Nat Neurosci 21:576–588 Available at: https://pubmed.ncbi.nlm.nih.gov/29556028/
607 [Accessed December 3, 2025].

608 Bareyre FM, Kerschensteiner M, Raineteau O, Mettenleiter TC, Weinmann O, Schwab ME (2004) The
609 injured spinal cord spontaneously forms a new intraspinal circuit in adult rats. Nat Neurosci 7:269–
610 277 Available at: https://pubmed.ncbi.nlm.nih.gov/14966523/ [Accessed December 10, 2025].

611 Battistuzzo CR, Callister RJ, Callister R, Galea MP (2012) A Systematic Review of Exercise Training To
612 Promote Locomotor Recovery in Animal Models of Spinal Cord Injury. J Neurotrauma 29:1600
613 Available at: https://pmc.ncbi.nlm.nih.gov/articles/PMC3353762/ [Accessed December 4, 2025].

614 Bonanno JL, O'Brien CF, Cafferty WBJ (2025) REVS: A new open-source platform for high-resolution
615 analysis of rodent wheel running behavior. J Neurosci Methods 424 Available at:
616 https://pubmed.ncbi.nlm.nih.gov/40946866/ [Accessed December 9, 2025].

617 Botta P, Fushiki A, Vicente AM, Hammond LA, Mosberger AC, Gerfen CR, Peterka D, Costa RM (2020)
618 An Amygdala Circuit Mediates Experience-Dependent Momentary Arrests during Exploration. Cell
619 183:605-619.e22 Available at: https://pubmed.ncbi.nlm.nih.gov/33031743/ [Accessed December 9,
620 2025].

621 Bradley PM, Denecke CK, Aljovic A, Schmalz A, Kerschensteiner M, Bareyre FM (2019) Corticospinal
622 circuit remodeling after central nervous system injury is dependent on neuronal activity. J Exp Med
623 216:2503–2514 Available at: https://pubmed.ncbi.nlm.nih.gov/31391209/ [Accessed December 9,
624 2025].

625 Brus-Ramer M, Carmel JB, Chakrabarty S, Martin JH (2007) Electrical Stimulation of Spared
626 Corticospinal Axons Augments Connections with Ipsilateral Spinal Motor Circuits after Injury. The

Journal of Neuroscience 27:13793 Available at: https://pmc.ncbi.nlm.nih.gov/articles/PMC6673617/ [Accessed December 3, 2025].

Burns AS, Marino RJ, Flanders AE, Flett H (2012) Clinical diagnosis and prognosis following spinal cord injury. Handb Clin Neurol 109:47–62 Available at: https://www.sciencedirect.com/science/chapter/handbook/pii/B9780444521378000036?via%3Dihub [Accessed December 4, 2025].

Cafferty WBJ, Strittmatter SM (2006) The Nogo-Nogo receptor pathway limits a spectrum of adult CNS axonal growth. J Neurosci 26:12242–12250 Available at: https://pubmed.ncbi.nlm.nih.gov/17122049/ [Accessed December 3, 2025].

Capelli P, Pivetta C, Esposito MS, Arber S (2017) Locomotor speed control circuits in the caudal brainstem. Nature 2017 551:7680 551:373–377 Available at: https://www.nature.com/articles/nature24064 [Accessed December 9, 2025].

Carmel JB, Berrol LJ, Brus-Ramer M, Martin JH (2010) Chronic electrical stimulation of the intact corticospinal system after unilateral injury restores skilled locomotor control and promotes spinal axon outgrowth. J Neurosci 30:10918–10926 Available at: https://pubmed.ncbi.nlm.nih.gov/20702720/ [Accessed December 10, 2025].

Carmel JB, Kimura H, Martin JH (2014) Electrical Stimulation of Motor Cortex in the Uninjured Hemisphere after Chronic Unilateral Injury Promotes Recovery of Skilled Locomotion through Ipsilateral Control. The Journal of Neuroscience 34:462 Available at: https://pmc.ncbi.nlm.nih.gov/articles/PMC3870931/ [Accessed December 3, 2025].

Carmona LM, Thomas ED, Smith K, Tasic B, Costa RM, Nelson A (2024) Topographical and cell type-specific connectivity of rostral and caudal forelimb corticospinal neuron populations. Cell Rep 43:113993 Available at: https://pmc.ncbi.nlm.nih.gov/articles/PMC11100358/ [Accessed December 3, 2025].

651 Chon U, Vanselow DJ, Cheng KC, Kim Y (2019) Enhanced and unified anatomical labeling for a
652 common mouse brain atlas. Nat Commun 10 Available at:
653 https://pubmed.ncbi.nlm.nih.gov/31699990/ [Accessed December 9, 2025].
654 Dancause N, Barbay S, Frost SB, Plautz EJ, Chen D, Zoubina E V., Stowe AM, Nudo RJ (2005)
655 Extensive cortical rewiring after brain injury. J Neurosci 25:10167–10179 Available at:
656 https://pubmed.ncbi.nlm.nih.gov/16267224/ [Accessed December 3, 2025].
657 Esposito MS, Capelli P, Arber S (2014) Brainstem nucleus MdV mediates skilled forelimb motor tasks.
658 Nature 508:351–356 Available at: https://pubmed.ncbi.nlm.nih.gov/24487621/ [Accessed December
659 9, 2025].
660 Filli L, Engmann AK, Zörner B, Weinmann O, Moraitis T, Gullo M, Kasper H, Schneider R, Schwab ME
661 (2014) Bridging the Gap: A Reticulo-Propriospinal Detour Bypassing an Incomplete Spinal Cord
662 Injury. The Journal of Neuroscience 34:13399 Available at:
663 https://pmc.ncbi.nlm.nih.gov/articles/PMC6608315/ [Accessed December 10, 2025].
664 Fink KL, Cafferty WBJ (2016) Reorganization of Intact Descending Motor Circuits to Replace Lost
665 Connections After Injury. Neurotherapeutics 13:370–381 Available at:
666 https://pubmed.ncbi.nlm.nih.gov/26846379/ [Accessed December 9, 2025].
667 Ghosh A, Sydekum E, Haiss F, Peduzzi S, Zörner B, Schneider R, Baltes C, Rudin M, Weber B, Schwab
668 ME (2009) Functional and anatomical reorganization of the sensory-motor cortex after incomplete
669 spinal cord injury in adult rats. J Neurosci 29:12210–12219 Available at:
670 https://pubmed.ncbi.nlm.nih.gov/19793979/ [Accessed December 3, 2025].
671 Girgis J, Merrett D, Kirkland S, Metz GAS, Verge V, Fouad K (2007) Reaching training in rats with
672 spinal cord injury promotes plasticity and task specific recovery. Brain 130:2993–3003 Available at:
673 https://pubmed.ncbi.nlm.nih.gov/17928316/ [Accessed December 9, 2025].
674 Glover IS, Baker SN (2022) Both Corticospinal and Reticulospinal Tracts Control Force of Contraction. J
675 Neurosci 42:3150–3164 Available at: https://pubmed.ncbi.nlm.nih.gov/35241490/ [Accessed
676 December 10, 2025].

677 Golan N, Ehrlich DB, Bonanno J, O'Brien RF, Murillo M, Kauer S, Ravindra N, van Dijk D, Cafferty
678 WBJ (2023) Anatomical Diversity of the Adult Corticospinal Tract Revealed by Single-Cell
679 Transcriptional Profiling. Journal of Neuroscience 43:7929–7945 Available at:
680 https://www.jneurosci.org/content/43/47/7929 [Accessed December 3, 2025].
681 Inoue T, Ueno M (2025) The diversity and plasticity of descending motor pathways rewired after stroke
682 and trauma in rodents. Front Neural Circuits 19 Available at:
683 https://pubmed.ncbi.nlm.nih.gov/40191711/ [Accessed December 9, 2025].
684 Iwaniuk AN, Whishaw IQ (2000) On the origin of skilled forelimb movements. Trends Neurosci 23:372–
685 376 Available at: https://pubmed.ncbi.nlm.nih.gov/10906801/ [Accessed December 9, 2025].
686 Jeleva R, Muhr CD, Liebisch AP, Bareyre FM (2026) Differential plasticity of excitatory and inhibitory
687 reticulospinal fibers after spinal cord injury: Implication for recovery. Neural Regen Res 21:2011–
688 2020 Available at: https://pubmed.ncbi.nlm.nih.gov/39995061/ [Accessed December 10, 2025].
689 Kleim JA, Jones TA (2008) Principles of experience-dependent neural plasticity: implications for
690 rehabilitation after brain damage. J Speech Lang Hear Res 51 Available at:
691 https://pubmed.ncbi.nlm.nih.gov/18230848/ [Accessed December 10, 2025].
692 Krajacic A, Weishaupt N, Girgis J, Tetzlaff W, Fouad K (2010) Training-induced plasticity in rats with
693 cervical spinal cord injury: Effects and side effects. Behavioural Brain Research 214:323–331
694 Available at: https://pubmed.ncbi.nlm.nih.gov/20573587/ [Accessed December 9, 2025].
695 LaPash Daniels CM, Ayers KL, Finley AM, Culver JP, Goldberg MP (2009) Axon sprouting in adult
696 mouse spinal cord after motor cortex stroke. Neurosci Lett 450:191–195 Available at:
697 https://www.researchgate.net/publication/23486380_Axon_sprouting_in_adult_mouse_spinal_cord_
698 after_motor_cortex_stroke [Accessed December 3, 2025].
699 Lee KE, Jeoung B (2023) An analysis of the effectiveness of rehabilitation protocols for patients with
700 spinal cord injury: A systematic review. Journal of Public Health 2023 33:7 33:1461–1470
701 Available at: https://link.springer.com/article/10.1007/s10389-023-02115-9 [Accessed December 4,
702 2025].

703 Lemieux M, Karimi N, Bretzner F (2024) Functional plasticity of glutamatergic neurons of medullary
704 reticular nuclei after spinal cord injury in mice. Nat Commun 15:1542 Available at:
705 https://pmc.ncbi.nlm.nih.gov/articles/PMC10879492/ [Accessed December 9, 2025].
706 Lemon RN, Griffiths J (2005) Comparing the function of the corticospinal system in different species:
707 organizational differences for motor specialization? Muscle Nerve 32:261–279 Available at:
708 https://pubmed.ncbi.nlm.nih.gov/15806550/ [Accessed December 3, 2025].
709 Liang H, Watson C, Paxinos G (2016) Terminations of reticulospinal fibers originating from the
710 gigantocellular reticular formation in the mouse spinal cord. Brain Struct Funct 221:1623–1633
711 Available at: https://pubmed.ncbi.nlm.nih.gov/25633472/ [Accessed December 9, 2025].
712 Lindau NT, Bänninger BJ, Gullo M, Good NA, Bachmann LC, Starkey ML, Schwab ME (2014)
713 Rewiring of the corticospinal tract in the adult rat after unilateral stroke and anti-Nogo-A therapy.
714 Brain 137:739–756 Available at: https://pubmed.ncbi.nlm.nih.gov/24355710/ [Accessed December
715 3, 2025].
716 Liu BP, Cafferty WBJ, Budel SO, Strittmatter SM (2006) Extracellular regulators of axonal growth in the
717 adult central nervous system. Philosophical Transactions of the Royal Society B: Biological
718 Sciences 361:1593–1610 Available at: https://dx.doi.org/10.1098/rstb.2006.1891 [Accessed
719 December 3, 2025].
720 Liu J, Yang XY, Xia WW, Dong J, Yang MG, Jiao JH (2016) Fine motor skill training enhances
721 functional plasticity of the corticospinal tract after spinal cord injury. Neural Regen Res 11:1990
722 Available at: https://pmc.ncbi.nlm.nih.gov/articles/PMC5270439/ [Accessed December 3, 2025].
723 Liu Y, Latremoliere A, Li X, Zhang Z, Chen M, Wang X, Fang C, Zhu J, Alexandre C, Gao Z, Chen B,
724 Ding X, Zhou JY, Zhang Y, Chen C, Wang KH, Woolf CJ, He Z (2018) Touch and tactile
725 neuropathic pain sensitivity are set by corticospinal projections. Nature 561:547–550 Available at:
726 https://pubmed.ncbi.nlm.nih.gov/30209395/ [Accessed December 10, 2025].

Loy K, Bareyre FM (2019) Rehabilitation following spinal cord injury: how animal models can help our understanding of exercise-induced neuroplasticity. Neural Regen Res 14:405 Available at: https://pmc.ncbi.nlm.nih.gov/articles/PMC6334617/ [Accessed December 4, 2025].

Loy K, Schmalz A, Hoche T, Jacobi A, Kreutzfeldt M, Merkler D, Bareyre FM (2018) Enhanced Voluntary Exercise Improves Functional Recovery following Spinal Cord Injury by Impacting the Local Neuroglial Injury Response and Supporting the Rewiring of Supraspinal Circuits. J Neurotrauma 35:2904–2915 Available at: https://www.liebertpub.com/doi/pdf/10.1089/neu.2017.5544?download=true [Accessed December 9, 2025].

Mathis A, Mamidanna P, Cury KM, Abe T, Murthy VN, Mathis MW, Bethge M (2018) DeepLabCut: markerless pose estimation of user-defined body parts with deep learning. Nature Neuroscience 2018 21:9 21:1281–1289 Available at: https://www.nature.com/articles/s41593-018-0209-y [Accessed December 9, 2025].

Mensah EO, Chalif JI, Johnston BR, Chalif E, Parker T, Izzy S, He Z, Saigal R, Fehlings MG, Lu Y (2025) Traumatic spinal cord injury: a review of the current state of art and future directions – what do we know and where are we going? North American Spine Society Journal (NASSJ) 22:100601 Available at: https://www.sciencedirect.com/science/article/pii/S2666548425000216 [Accessed December 4, 2025].

Metz GA, Whishaw IQ (2009) The ladder rung walking task: a scoring system and its practical application. J Vis Exp Available at: https://pubmed.ncbi.nlm.nih.gov/19525918/ [Accessed December 9, 2025].

Moreno-Lopez Y, Bichara C, Delbecq G, Isope P, Cordero-Erausquin M (2021) The corticospinal tract primarily modulates sensory inputs in the mouse lumbar cord. Elife 10 Available at: https://pubmed.ncbi.nlm.nih.gov/34497004/ [Accessed December 10, 2025].

751 Nelson A, Abdelmesih B, Costa RM (2021) Corticospinal populations broadcast complex motor signals
752 to coordinated spinal and striatal circuits. Nat Neurosci 24:1721–1732 Available at:
753 https://pubmed.ncbi.nlm.nih.gov/34737448/ [Accessed December 3, 2025].
754 Oudega M, Perez MA (2012) Corticospinal reorganization after spinal cord injury. J Physiol 590:3647
755 Available at: https://pmc.ncbi.nlm.nih.gov/articles/PMC3476625/ [Accessed December 3, 2025].
756 Raineteau O, Schwab ME (2001) Plasticity of motor systems after incomplete spinal cord injury. Nat Rev
757 Neurosci 2:263–273 Available at: https://pubmed.ncbi.nlm.nih.gov/11283749/ [Accessed December
758 4, 2025].
759 Siegel CS, Fink KL, Strittmatter SM, Cafferty WBJ (2015) Plasticity of intact rubral projections mediates
760 spontaneous recovery of function after corticospinal tract injury. J Neurosci 35:1443–1457
761 Available at: https://pubmed.ncbi.nlm.nih.gov/25632122/ [Accessed December 9, 2025].
762 Starkey ML, Bleul C, Maier IC, Schwab ME (2011) Rehabilitative training following unilateral
763 pyramidotomy in adult rats improves forelimb function in a non-task-specific way. Exp Neurol
764 232:81–89 Available at: https://pubmed.ncbi.nlm.nih.gov/21867701/ [Accessed December 3, 2025].
765 Ueno M, Hayano Y, Nakagawa H, Yamashita T (2012) Intraspinal rewiring of the corticospinal tract
766 requires target-derived brain-derived neurotrophic factor and compensates lost function after brain
767 injury. Brain 135:1253–1267 Available at: https://pubmed.ncbi.nlm.nih.gov/22436236/ [Accessed
768 December 9, 2025].
769 Ueno M, Nakamura Y, Li J, Gu Z, Niehaus J, Maezawa M, Crone SA, Goulding M, Baccei ML, Yoshida
770 Y (2018) Corticospinal Circuits from the Sensory and Motor Cortices Differentially Regulate
771 Skilled Movements through Distinct Spinal Interneurons. Cell Rep 23:1286-1300.e7 Available at:
772 https://www.cell.com/action/showFullText?pii=S2211124718305254 [Accessed December 10,
773 2025].
774 Van Steenbergen V, Burattini L, Trumpp M, Fourneau J, Aljović A, Chahin M, Oh H, D'ambra M,
775 Bareyre FM (2022) Coordinated neurostimulation promotes circuit rewiring and unlocks recovery

after spinal cord injury. J Exp Med 220:e20220615 Available at: https://pmc.ncbi.nlm.nih.gov/articles/PMC9794600/ [Accessed December 3, 2025].

Wagner FB et al. (2018) Targeted neurotechnology restores walking in humans with spinal cord injury. Nature 563:65–93 Available at: https://pubmed.ncbi.nlm.nih.gov/30382197/ [Accessed December 3, 2025].

Wahl AS, Omlor W, Rubio JC, Chen JL, Zheng H, Schröter A, Gullo M, Weinmann O, Kobayashi K, Helmchen F, Ommer B, Schwab ME (2014) Asynchronous therapy restores motor control by rewiring of the rat corticospinal tract after stroke. Science (1979) 344:1250–1255 Available at: /doi/pdf/10.1126/science.1253050?download=true [Accessed December 10, 2025].

Wang Z, Romanski A, Mehra V, Wang Y, Brannigan M, Campbell BC, Petsko GA, Tsoulfas P, Blackmore MG (2022) Brain-wide analysis of the supraspinal connectome reveals anatomical correlates to functional recovery after spinal injury. Elife 11:e76254 Available at: https://pmc.ncbi.nlm.nih.gov/articles/PMC9345604/ [Accessed December 10, 2025].

Weidner N, Ner A, Salimi N, Tuszynski MH (2001) Spontaneous corticospinal axonal plasticity and functional recovery after adult central nervous system injury. Proc Natl Acad Sci U S A 98:3513–3518 Available at: https://www.pnas.org/doi/pdf/10.1073/pnas.051626798 [Accessed December 3, 2025].

Zhang Z et al. (2024) Spinal projecting neurons in rostral ventromedial medulla co-regulate motor and sympathetic tone. Cell 187:3427-3444.e21 Available at: https://pubmed.ncbi.nlm.nih.gov/38733990/ [Accessed December 9, 2025].

800 **Figure Legends**

801 **Figure 1. Mice with uPyX engage in significant voluntary complex wheel running**
802 **rehabilitation.** Mice had access to wheels for voluntary rehabilitation for 26 days post-lesion
803 **(A).** Schematic of uPyX **(B)** and representative histological verifications of a sham and uPyX
804 animals are shown **(C, C')**. Wheel running data was collected using the REVs platform (**D**).
805 Representative image of a mouse running, with inset showing forelimb rung grasping (**E**). Side-
806 profile of mouse running **(F)**. Mean runtime from baseline to 28 dpi showed an acute deficit as
807 revealed by an interaction effect between lesion and day ($F_{(2,374)} = 5.295$, $p < 0.0001$, ANOVA).
808 Bonferroni-corrected post hoc testing revealed a significant difference at 2 dpi ($p=0.01$, t-test)
809 **(G)**. Mean speed **(H)** and distance **(I)** also showed significant interaction effects (speed: ($F_{(2,374)} =$
810 4.469, $p < 0.0001$; distance: ($F_{(2,374)} = 5.552$, $p < 0.0001$; ANOVAs) and deficits at 2 dpi (speed:
811 $p = 0.03$; distance: $p = 0.00006$; t-tests). Total cumulative distance ultimately showed no
812 difference between lesioned and sham mice ($F_{(1,17)}=0.990$, $p=0.334$, ANOVA) **(J)**. Dotted red
813 line indicates lesion timepoint, 0 dpi. * = $p < 0.01$, *** = $p < 0.001$. Scale bar = 200 µm.
814

815 **Figure 2. Rehabilitation promotes forelimb fine motor function recovery in uPyX mice.**
816 Complex ladder rung testing was completed on -2, 2, 7, 14, 21, and 28 dpi **(A)**. Representative
817 image of a mouse crossing the complex ladder with examples of quantified errors **(B)**. Total
818 number of injured forelimb (FL) steps significantly increased in lesioned animals ($F_{(1,33)} =$
819 14.445, $p = 0.0006$, ANOVA). This lesion effect persisted through 28 dpi ($F_{(1,32)} = 13.339$, $p =$
820 0.0009, ANOVA), but there was no effect of rehabilitation ($F_{(1,32)} = 0.772$, $p = 0.402$, ANOVA)
821 (**C**). Injured FL footfalls significantly increased in lesioned animals ($F_{(1,33)} = 20.782$, $p =$
822 0.00007, ANOVA) and this lesion effect persisted through 28 dpi ($F_{(1,32)} = 12.090$, $p = 0.001$,

823 ANOVA). There was additionally a significant effect of rehabilitation ($F_{(1,32)} = 7.938$ $p = 0.008$,
824 ANOVA). Bonferroni-corrected post hoc tests revealed a trend of uPyX+Rehab having improved
825 performance relative to uPyX-Rehab at 7 dpi ($p = 0.071$, t-test) and 14 dpi ($p = 0.052$, t-test).
826 There was a significant difference between the two groups at 21 dpi ($p = 0.003$, t-test) and 28 dpi
827 ($p = 0.035$, t-test) **(D)**. The intact FL also showed a significant lesion-induced footfall deficit
828 ($F_{(1,33)} = 4.719$, $p = 0.037$, ANOVA) at 2 dpi, but it did not persist through 28 dpi ($F_{(1,32)} = 2.186$,
829 $p = 0.149$, ANOVA). Although there was no long-term lesion effect, there was a main effect of
830 rehabilitation ($F_{(1,32)} = 4.37$, $p = 0.045$, ANOVA) **(E)**. The injured FL had a significant increase
831 in reach errors at 2 dpi ($F_{(1,33)} = 15.125$, $p = 0.00046$, ANOVA). This effect persisted through 28
832 dpi ($F_{(1,32)} = 11.483$, $p = 0.002$, ANOVA), and there was additionally a significant effect of
833 rehabilitation ($F_{(1,32)} = 9.171$, $p = 0.005$, ANOVA). Bonferroni-corrected post hoc tests revealed
834 that uPyX+Rehab significantly improved performance relative to uPyX-Rehab for injured FL
835 reaches at 7 dpi ($p = 0.00178$, t-test), 14 dpi ($p = 0.0114$, t-test), 21 dpi ($p = 0.00296$, t-test), and
836 28 dpi ($p = 0.00943$, t-test) **(F)**. Injured HL footfalls had a significant lesion-induced increase at
837 2 dpi ($F_{(1,33)} = 10.603$, $p = 0.003$, ANOVA), which persisted through 28 dpi ($F_{(1,32)} = 9.558$, $p =$
838 0.004, ANOVA). There was a trend of rehabilitation improving injured HL footfalls ($F_{(1,32)} =$
839 3.347, $p = 0.077$, ANOVA) **(G)**. Intact HL footfalls significantly increased with lesion at 2 dpi
840 ($F_{(1,33)} = 4.317$, $p = 0.046$, ANOVA) and this effect persisted through 28 dpi ($F_{(1,33)} = 4.506$, $p =$
841 0.042, ANOVA). There was a trend of rehabilitation improving intact HL footfalls ($F_{(1,32)} =$
842 3.510, $p = 0.070$, ANOVA) **(H)**. Principal component analyses revealed that all 4 groups
843 clustered together at -2 dpi **(I)**. At 2 dpi, the two lesion groups separated from the sham groups,
844 driven most strongly by differences in cross time, step count, and injured FL errors **(J)**. By 28

845 dpi, the uPyX+Rehab separated from uPyX-Rehab and re-clustered with the sham groups **(K)**. *
846 = $p < 0.05$, = $p<0.10$.
847
848 **Figure 3. Rehabilitation functionally recruits intact CSNs.** Schematic of intersectional tracing
849 approach to target CSNs for labeling in M2 and M1 of mouse cortex **(A)**. There was a significant
850 main effect of rehabilitation on percentage of cFos+ CSNs in M2, with rehab groups showing an
851 increased colocalization (p=0.00538, linear mixed-effect model). Filled and open circles
852 represent values from CFA- and RFA- traced cells respectively **(B)**. Representative images of
853 M2 CSN and c-Fos labeling. Red arrows indicate a c-Fos- CSN and white arrows indicate a c-
854 Fos+ CSN **(C, D)**. There was a significant main effect of rehabilitation on percentage of c-Fos+
855 CSNs in M1, with rehab groups showing increased colocalization (p=0.00389, linear mixed-
856 effect model). Filled and open circles represent values from CFA- and RFA- traced cells
857 respectively **(E)**. There was no effect of tracing origin on c-fos activation for both M2 (p=0.142,
858 linear mixed-effect model) and M1 (p=0.079, linear mixed-effect model). Representative images
859 of M1 CSN and c-Fos labeling. Green arrows indicate a c-Fos- CSN and white arrows indicate a
860 c-Fos+ CSN **(F, G)**. Scale bar = 100 microns. *** = $p < 0.001$.
861
862 **Figure 4. Large-scale reorganization of intact corticospinal tract projections in the lesioned**
863 **and rehabilitated mouse brain.** Representative intact corticospinal tract projections at 0.0 AP, -
864 2.0 AP, -4.0 AP, and -6.0 AP from bregma. High-level organization of mouse brain regions are
865 color-coded: blue = cerebrum, interbrain = green, midbrain = purple, pons = orange, medulla =
866 pink, cerebellum = yellow. Traced projections are shown in black **(A)**. Quantification of
867 normalized projection density in 15 functional subregions in control, uPyX-Rehab, and

868 uPyX+Rehab mice. Closed and open circles represent values from CFA- and RFA- traced CSNs
869 respectively. There was no significant effect of tracing origin on projection density (p=0.2447,
870 linear mixed-effect model). The uPyX+Rehab mice had reduced projection density in the non-
871 motor isocortex compared to control animals (p = 0.005587, linear mixed-effect model). uPyX-
872 Rehab and uPyX+Rehab had increased projection density in the motor medulla compared to
873 control animals (uPyX-Rehab vs. control, p = 0.0129; uPyX+Rehab vs. control, p = 0.000031;
874 linear mixed-effect models). There were no significant differences in the other regions. **(B)**.
875 Correlation between Rehabilitation Index and Plasticity Index for spinally-projecting medulla-
876 motor regions in uPyX+Rehab and uPyX-Rehab mice. There was a significant correlation in
877 uPyX+Rehab mice ($R^2 = 0.161$, p = 0.0341, Pearson's correlation), but not uPyX-Rehab mice
878 ($R^2 = 0.004$, p = 0.762, Pearson's correlation) **(C, D)**. In spinally-projecting pons-motor regions,
879 there were no significant correlations in uPyX+Rehab ($R^2 = 0.03$, p = 0.399, Pearson's
880 correlation), nor uPyX-Rehab animals ($R^2 = 0.002$, p = 0.811, Pearson's correlation). Filled and
881 open circles represent values from CFA- and RFA- traced cells respectively **(E, F)**. * = $p < 0.05$,
882 ** = $p < 0.01$, *** = $p < 0.001$. Thal-sm=Sensory-motor thalamus, Thal-other=Thalamus other,
883 Hyp=Hypothalamus, Mb-mot=Motor midbrain, Mb-sen=Sensory midbrain, Mb-other=Midbrain
884 other, P-mot=Motor pons, P-sen=Sensory pons, P-other=Pons other, My-mot=Motor medulla,
885 My-sen=Sensory medulla, My-other=medulla other, Cb-nuc=Cerebellar nuclei.
886
887 **Figure 5. Subregion specific reorganization of intact corticospinal tract projections in the**
888 **lesioned and rehabilitated (reticular formation) mouse brain.** Normalized projection density
889 increased in the lateral paragigantoreticular nucleus (LPGi) of uPyX+Rehab mice compared to
890 control mice (t=2.91, p=0.01, Tukey-adjusted post hoc). There was no main effect of tracing

origin (t=0.850, p=0.408; linear mixed-effect model) **(A)**. Normalized projection density increased in both uPyX+Rehab (t = 6.67, p < 0.0001, Tukey-adjusted post hoc) mice compared to controls, and uPyX+Rehab mice compared to uPyX-Rehab mice (t = 3.98, p = 0.002, Tukey-adjusted t-test) in the alpha part of the gigantoreticular nucleus (GiA). There was no main effect of tracing origin (t=0.851, p=0.407; linear mixed-effect model) **(B)**. Normalized projection density increased in both uPyX+Rehab (t = 7.11, p < 0.0001, Tukey-adjusted post hoc) mice compared to controls, and uPyX+Rehab mice compared to uPyX-Rehab mice (t = 3.70, p = 0.001706, Tukey-adjusted t-test) in the ventral part of the medullary reticular nucleus (MdV). Normalized projection density also increased in uPyX-Rehab mice compared to controls (t = 3.34, p = 0.004967, Tukey-adjusted t-test). There was no main effect of tracing origin (t=1.493, p=0.157; linear mixed-effect model) **(C)**. Schematic of the rostral medulla (**D**) and representative images of intact CST density in a control **(E)**, uPyX-Rehab **(F)**, and uPyX+Rehab **(G)** mouse. Schematic of the caudal medulla **(H)** and representative images of intact CST density in a control **(I)**, uPyX-Rehab **(J)**, and uPyX+Rehab **(K)** mouse. The red box indicates the zoomed-in area of interest. Correlations between percentage of injured forelimb footfall recovery and normalized projection density were not significant in the LPGi ($R^2 = 0.012$, p = 0.654, Pearson's correlation) nor GiA ($R^2 = 0.087$, p = 0.221, Pearson's correlation) **(L, M)**. Correlation between percentage of injured forelimb footfall recovery and normalized projection density was significant in the MdV ($R^2 = 0.327$, p = 0.0105, Pearson's correlation). Closed and open circles represent values from CFA- and RFA- traced CSNs respectively **(N)**. * = p < 0.05, ** = p < 0.01, *** = p < 0.001. Scale bar = 200 microns.

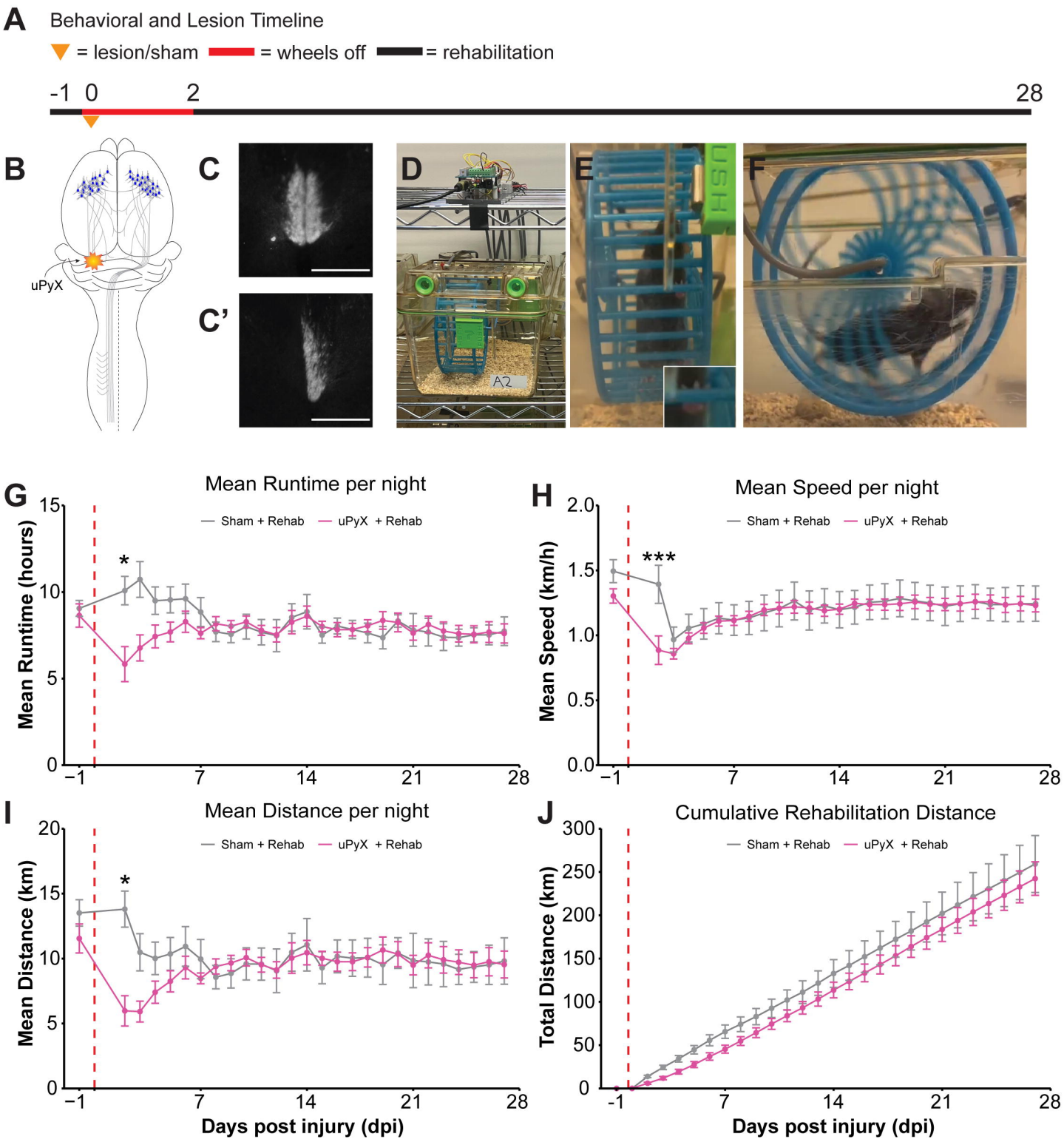
A
Behavioral and Lesion Timeline
= lesion/sham
= wheels off
= rehabilitation
-1
0
2
28
B
uPyX
C
C'
D
A2
E
F
G
Mean Runtime per night
Sham + Rehab
uPyX + Rehab
Mean Runtime (hours)
*
H
Mean Speed per night
Mean Speed (km/h)
***
I
Mean Distance per night
Mean Distance (km)
Days post injury (dpi)
J
Cumulative Rehabilitation Distance
Total Distance (km)
Days post injury (dpi)

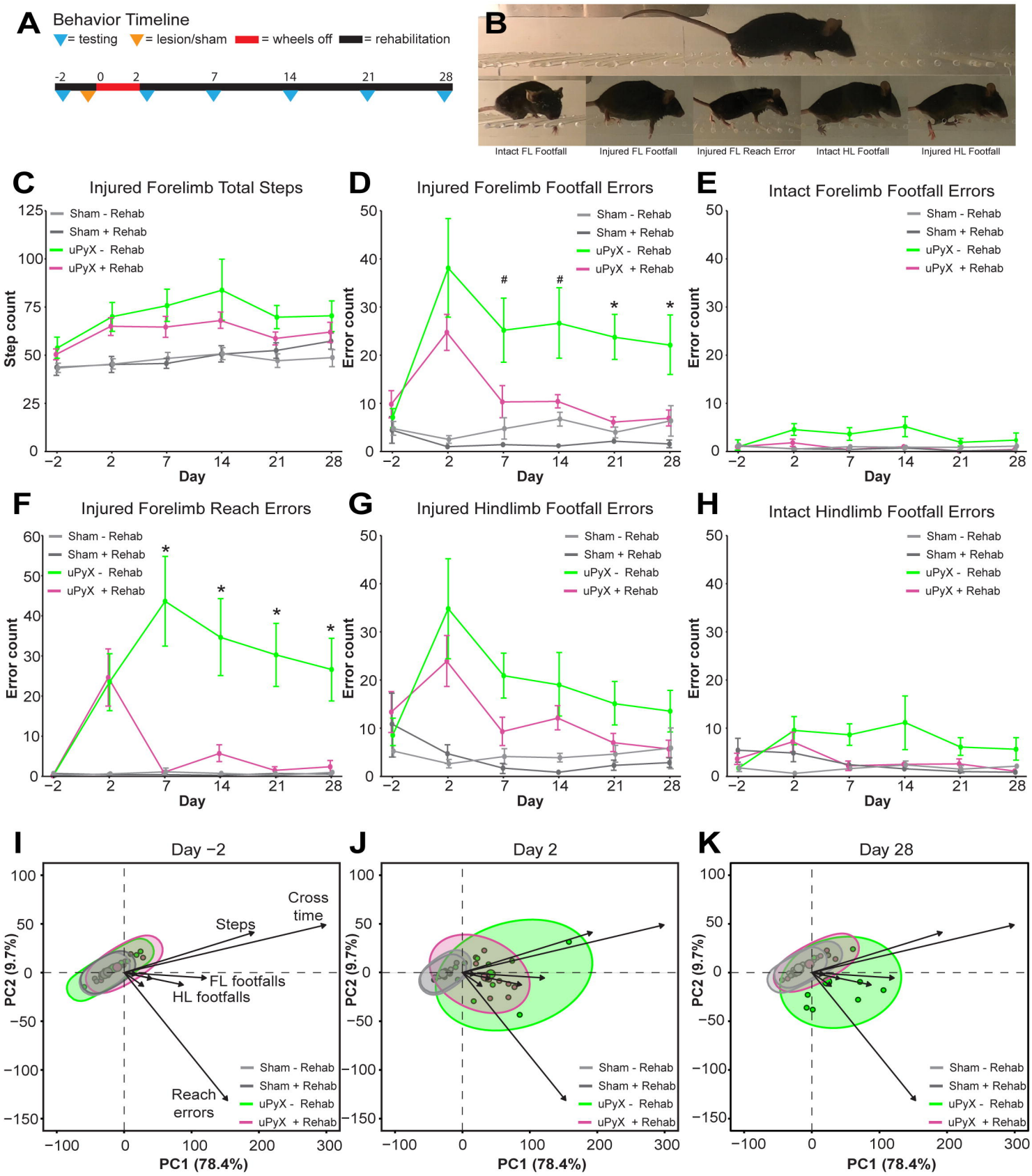
A
Behavior Timeline
= testing
= lesion/sham
= wheels off
= rehabilitation
-2
0
2
7
14
21
28
B
Intact FL Footfall
Injured FL Footfall
Injured FL Reach Error
Intact HL Footfall
Injured HL Footfall
C
Injured Forelimb Total Steps
Step count
Day
D
Injured Forelimb Footfall Errors
Error count
Day
E
Intact Forelimb Footfall Errors
Error count
Day
F
Injured Forelimb Reach Errors
Error count
Day
G
Injured Hindlimb Footfall Errors
Error count
Day
H
Intact Hindlimb Footfall Errors
Error count
Day
Sham - Rehab
Sham + Rehab
uPyX - Rehab
uPyX + Rehab
I
Day −2
J
Day 2
K
Day 28
Cross time
Steps
FL footfalls
HL footfalls
Reach errors
PC1 (78.4%)
PC2 (9.7%)

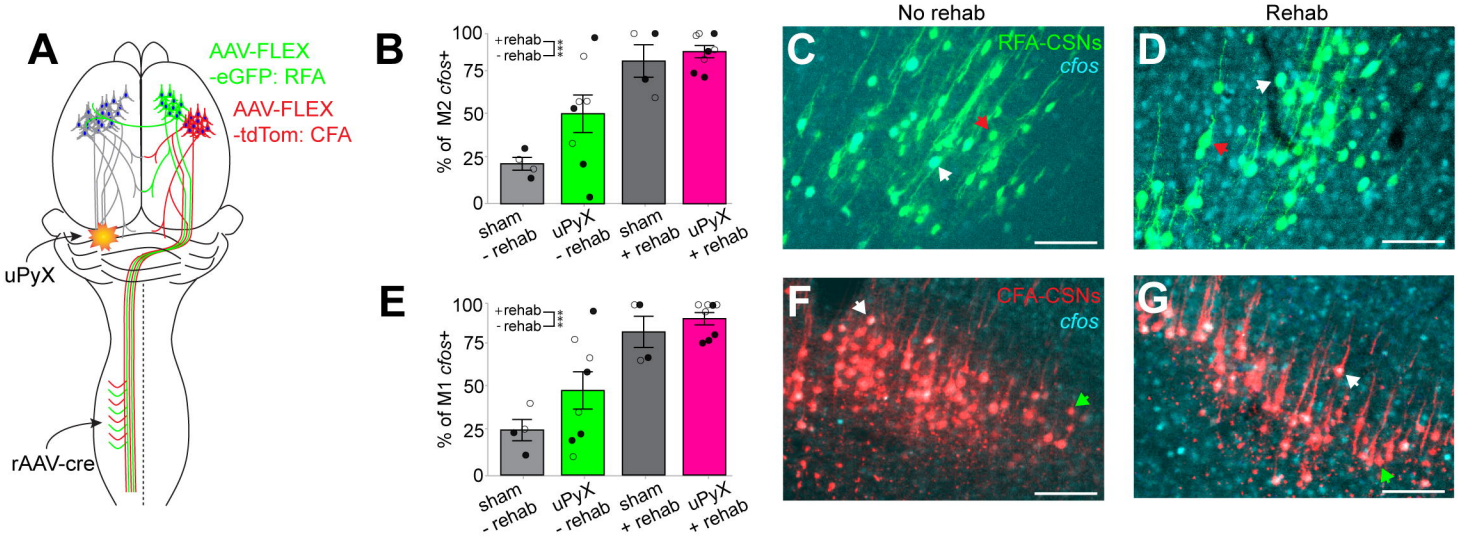
A
AAV-FLEX
-eGFP: RFA
AAV-FLEX
-tdTom: CFA
uPyX
rAAV-cre
B
% of M2 cfos+
+rehab
-rehab
***
sham - rehab
uPyX - rehab
sham + rehab
uPyX + rehab
E
% of M1 cfos+
No rehab
Rehab
C
RFA-CSNs
cfos
D
F
CFA-CSNs
cfos
G

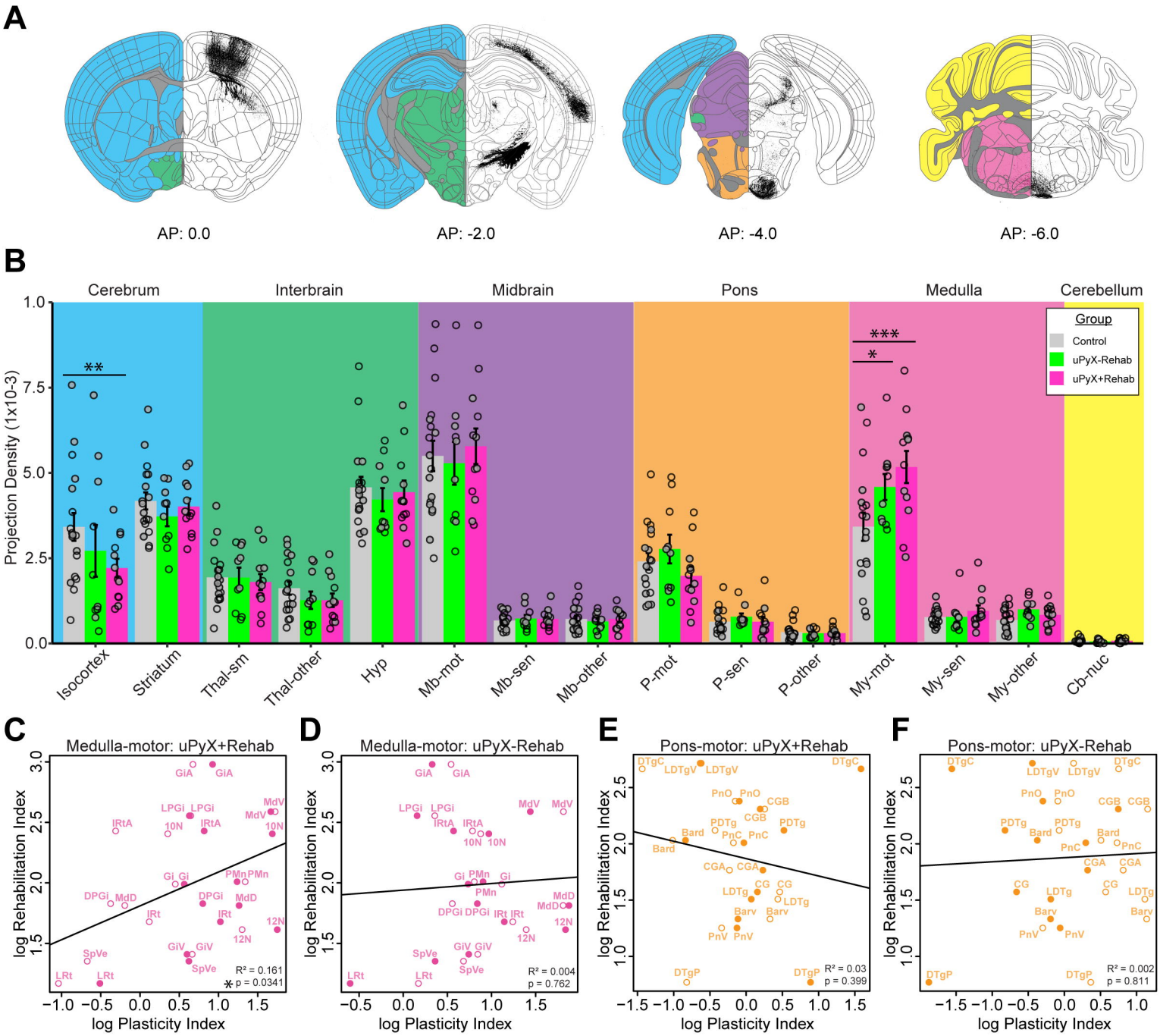
A
AP: 0.0
AP: -2.0
AP: -4.0
AP: -6.0
B
Cerebrum
Interbrain
Midbrain
Pons
Medulla
Cerebellum
Projection Density (1x10-3)
Group
Control
uPyX-Rehab
uPyX+Rehab
Isocortex
Striatum
Thal-sm
Thal-other
Hyp
Mb-mot
Mb-sen
Mb-other
P-mot
P-sen
P-other
My-mot
My-sen
My-other
Cb-nuc
C
Medulla-motor: uPyX+Rehab
R² = 0.161
p = 0.0341
D
Medulla-motor: uPyX-Rehab
R² = 0.004
p = 0.762
E
Pons-motor: uPyX+Rehab
R² = 0.03
p = 0.399
F
Pons-motor: uPyX-Rehab
R² = 0.002
p = 0.811
log Rehabilitation Index
log Plasticity Index

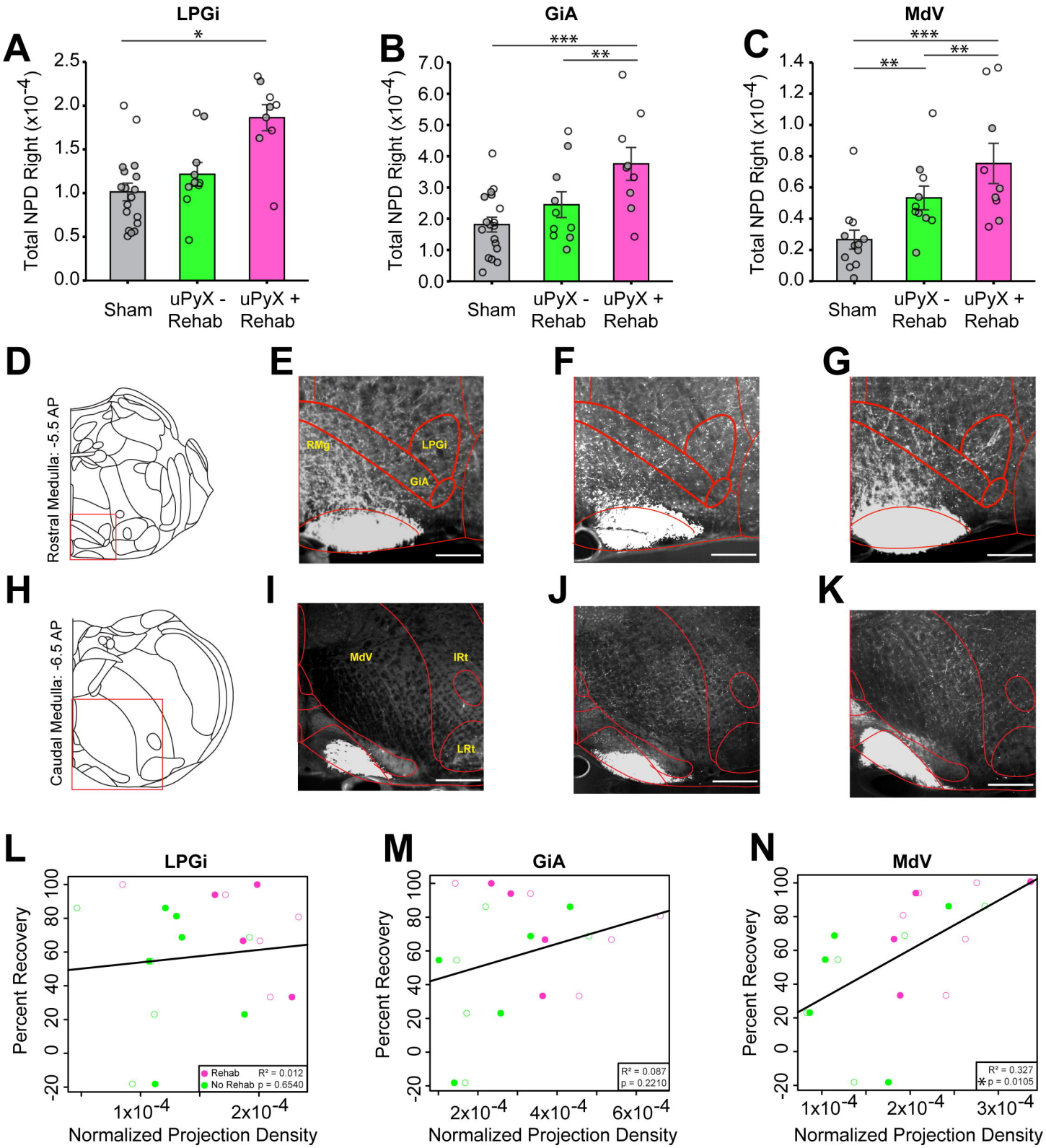
A
LPGi
*
Total NPD Right (x10^-4)
2.5
2.0
1.5
1.0
0.5
0.0
Sham
uPyX - Rehab
uPyX + Rehab
B
GiA
***
**
7.0
6.0
5.0
4.0
3.0
2.0
1.0
0.0
C
MdV
***
**
**
1.4
1.2
1.0
0.8
0.6
0.4
0.2
0.0
D
Rostral Medulla: -5.5 AP
E
RMg
LPGi
GiA
F
G
H
Caudal Medulla: -6.5 AP
I
MdV
IRt
LRt
J
K
L
LPGi
Percent Recovery
100
80
60
40
20
0
-20
Rehab R² = 0.012
No Rehab p = 0.6540
1x10^-4
2x10^-4
Normalized Projection Density
M
GiA
R² = 0.087
p = 0.2210
2x10^-4
4x10^-4
6x10^-4
N
MdV
R² = 0.327
* p = 0.0105
3x10^-4